

# Final-state interaction and recoil polarization in $(e, e'p)$ reactions: comparison with the polarized target case

J.E. Amaro<sup>1</sup>, J.A. Caballero<sup>2</sup>, T.W. Donnelly<sup>3</sup>, F. Kazemi Tabatabaei<sup>1</sup>

<sup>1</sup> *Departamento de Física Moderna, Universidad de Granada, Granada 18071, Spain*

<sup>2</sup> *Departamento de Física Atómica, Molecular y Nuclear, Universidad de Sevilla, Apdo. 1065, Sevilla 41080, Spain*

<sup>3</sup> *Center for Theoretical Physics, Laboratory for Nuclear Science and Department of Physics, Massachusetts Institute of Technology, Cambridge, MA 02139, USA*

---

## Abstract

A study of the total cross section for polarized proton knockout in  $(e, e'p)$  reactions is carried out for the closed-shell nucleus  $^{40}\text{Ca}$ . The dependence of FSI effects on polarization observables viewed as functions of the nucleon polarization angles is analyzed and interpreted within the basis of a semi-classical model for the orbit of the struck nucleon and trajectory of the ejected nucleon. A comparison with the case of a  $^{39}\text{K}$  polarized target and unpolarized protons is performed.

---

*PACS:* 25.30.Fj; 24.10.Eq; 24.70.+s

*Keywords:* electromagnetic nucleon knockout; nucleon recoil polarization; polarized target; final-state interactions.

# 1 Introduction

In recent years the study of recoil polarization observables in  $(e, e'\vec{p})$  and  $(\vec{e}, e'\vec{p})$  reactions has attracted attention both from the experimental [1, 2] and theoretical [3, 4, 5, 6, 7, 8, 9, 10, 11, 12] points of view. In particular, many of the latest studies have been focused on the polarization transfer asymmetry in reactions initiated by polarized electrons [13, 14, 15, 16]. For these significant effort is being expended in investigations of light nuclei, with much of the focus being placed on the analysis of the polarization transfer in the  ${}^4\text{He}(\vec{e}, e'\vec{p}){}^3\text{H}$  reaction which has recently been measured at MAMI [17, 18]. One of the goals of such studies is to obtain information from the measured polarization transfer ratios about medium modifications of the proton form factor.

In the case of medium-weight nuclei the measurement of recoil nucleon polarization provides valuable information which is complementary to that obtained with unpolarized ejectiles [3, 4, 19, 20, 21]. Two experiments have been performed to date, both for quasielastic kinematics. In one of them [2], using polarized electrons, the polarization transfer  $P'_l, P'_s$  and ratio were measured for proton knockout from the various shells of  ${}^{16}\text{O}$  and high momentum transfer  $q = 1 \text{ GeV}/c$ . In the other [1], with unpolarized electrons, the induced normal polarization  $P_n$  was determined for the two shells of  ${}^{12}\text{C}$ , and a lower value of the momentum transfer,  $q \simeq 760 \text{ MeV}/c$ . The agreements reached with the experimental data using different Distorted-Wave Impulse Approximation (DWIA) models [6, 9, 10, 11, 12, 15] make these studies promising. The polarization observables provide a clean tool to study reaction mechanisms, nuclear structure details and electromagnetic properties of the system, and to disentangle the various theoretical ingredients contained in each model, since, being ratios of response functions, no ambiguities arise due to spectroscopic factors that have to be fitted to data. In particular, note that adequate modeling of the final-state interaction (FSI) is essential for a proper description of so-called Time-Reversal Odd (TRO) observables [20] such as the induced polarization, since they would be exactly zero in absence of FSI.

In this paper we are mainly interested in the polarization observables induced by *unpolarized* electrons, specifically reactions of the type  $(e, e'\vec{N})$  — in this work only the case  $N = p$  will be considered, but the formalism is also applicable to the case  $N = n$ . These are also TRO observables and, as stated above, they only arise in the presence of FSI, in contrast to the polarization transfer observables produced by polarized electrons, which are Time-Reversal Even (TRE) and are already different from zero in the Plane-Wave Impulse Approximation (PWIA). When the initial electron and target are unpolarized, the electron can hit with equal probability nucleons having all spin orientations at different places along its orbit. In absence of FSI these nucleons leave the nucleus as plane waves with the same amplitude, hence carrying no net induced polarization.

The mechanisms by which the FSI induce recoil polarization are mainly i) the absorption due to the imaginary part of the optical potential and ii) the spin-orbit interaction.

The first mechanism is similar to the one found in quasielastic proton scattering (News polarization [22, 23], Maris effect [24]). In these reactions the dominance of one side of the nucleus (with respect to the final momentum of the nucleon,  $\mathbf{p}'$ ) emphasizes a definite orientation of the initial orbit, and then also favors a definite orientation of the nucleon spin. An analogous effect was independently predicted for  $(e, e'p)$  reactions from polarized nuclei in [25]. Therein the effects of FSI on the cross section were shown to depend strongly on the nuclear orientation. This result was interpreted by a semi-classical picture of the reaction: for a given polarized shell and given missing momentum,  $\mathbf{p} = \mathbf{p}' - \mathbf{q}$ , the most probable value of the nucleon position can be determined, and from that one can evaluate the amount of nuclear matter that is crossed by the nucleon; this in turn can be related with the strength of absorption due to the imaginary part of the optical potential.

The results found in [25] and later extended to polarized electrons in [26] provide a clear geometric picture of these reactions on polarized nuclei. One of the aims of the present paper is to investigate the degree to which this picture can be extended to the case of induced nucleon polarization in  $(e, e'\vec{p})$  reactions with unpolarized targets. Results for the induced polarization in such reactions have already been interpreted in terms of the Maris effect in [1, 3]. In this paper we go in some depth into this interpretation of nucleon recoil polarization in the light of the results already found for polarized nuclei. We depend on the fact that effects beyond the impulse approximation arising from two-body meson exchange currents do not affect the present results for the  $(e, e'p)$  cross section for low missing momentum and quasielastic kinematics [11, 12], which is the region where the semi-classical picture can safely be applied. In particular, in this paper we want to bring out the differences found between observables which occur for polarizations in the initial state (target) and in the final state (recoil nucleon), and to highlight the advantages of one reaction over the other, as this can help to guide future polarization experiments.

In this sense the present study is complementary to work in progress focused on the more general case of polarization observables which occur when *both* target and ejectile are polarized [27]. Analyses of the complete set of polarization observables in  $(e, e'p)$  only exist for the case of light nuclei, in particular deuterium [28]–[33, 34], but not for medium-weight nuclei. In the present paper we apply the DWIA model of [11, 12, 35] to describe proton knockout from the  $d_{3/2}$  shell of  $^{40}\text{Ca}$  for various recoil polarization directions, and compare the results with those found for the model of [25, 26, 36] of proton knockout from the same shell of polarized  $^{39}\text{K}$ .

The structure of the paper is as follows: in Sec. 2 we briefly present the general formalism for  $(e, e'\vec{p})$  recoil polarization reactions which will serve as a basis for our DWIA model. In Sec. 3 we give results for the cross section for different polarizations of the proton and interpret these using the semi-classical picture of nucleon orbit. Connections are made there to the case of a polarized target. We also present results for other polarization observables — in particular the separated response functions. Finally the conclusions are presented in Sec. 4.

## 2 Formalism for $(e, e'\vec{p})$ reactions

In this section we present the basic formalism for  $(e, e'\vec{p})$  reactions on which the DWIA results of the next section are based. We closely follow the pioneering work on polarization observables developed in [20, 37, 38]. For brevity here we just give the basic required expressions; more details about our model can be found in our previous work [11, 39] and references therein.

The kinematics of the reaction are shown in Fig. 1. An electron with four-momentum  $K_e^\mu = (\epsilon_e, \mathbf{k}_e)$  scatters off a nucleus  $|A\rangle$  to final four-momentum  $K_e'^\mu = (\epsilon'_e, \mathbf{k}'_e)$ , and is detected in coincidence with a proton with momentum  $\mathbf{p}'$ . The residual nucleus is left in the discrete state  $|B\rangle$ . The energy transfer is  $\omega = \epsilon_e - \epsilon'_e$ . The proton polarization is measured in the direction  $\vec{s}$ . In this work we express the vector components in the Lab coordinate system where the  $z$ -axis points along the  $\mathbf{q}$  direction, with  $\mathbf{q} = \mathbf{k}_e - \mathbf{k}'_e$  the momentum transfer. The  $x$ -axis points along the transverse component of  $\mathbf{k}_e$  (perpendicular to  $\mathbf{q}$ ), together with  $z$  defining the scattering plane. The  $y$ -axis is perpendicular to that plane. The final momentum  $\mathbf{p}'$  of the proton with polar angles  $(\theta', \phi')$  together with the momentum transfer determines the reaction plane, which forms an angle  $\phi'$  with the scattering plane. Experimentally the nucleon polarization components are measured with respect to the barycentric system, which we also show in Fig. 1 for future reference. The two directions longitudinal ( $\vec{l}$ ) and sideways ( $\vec{t}$ ) lie in the reaction plane, while the normal direction ( $\vec{n}$ ) is perpendicular to it.

The  $(e, e'\vec{p})$  cross section for protons polarized in the  $\vec{s}$  direction may be written as

$$\Sigma \equiv \frac{d\sigma}{d\epsilon'_e d\Omega'_e d\Omega'} = K\sigma_M \left( v_L R^L + v_T R^T + v_{TL} R^{TL} + v_{TT} R^{TT} \right), \quad (1)$$

where  $\Omega'_e$  and  $\Omega'$  are the solid angles of the final electron and proton, respectively,  $\sigma_M$  is the Mott cross section and  $K = m_N p' / (2\pi\hbar)^3$ , with  $m_N$  the nucleon mass. The electron kinematical factors  $v_K$  are given by

$$v_L = \frac{Q^4}{q^2}, \quad v_T = \tan^2 \frac{\theta}{2} - \frac{Q^2}{2q^2} \quad (2)$$

$$v_{TT} = \frac{Q^2}{2q^2}, \quad v_{TL} = \frac{1}{\sqrt{2}} \frac{Q^2}{q^2} \sqrt{\tan^2 \frac{\theta}{2} - \frac{Q^2}{q^2}}, \quad (3)$$

with  $Q^2 = \omega^2 - q^2 < 0$ . Finally the exclusive nuclear responses are the following components

$$R^L = W^{00}, \quad R^T = W^{xx} + W^{yy} \quad (4)$$

$$R^{TL} = \sqrt{2} (W^{0x} + W^{x0}), \quad R^{TT} = W^{yy} - W^{xx} \quad (5)$$

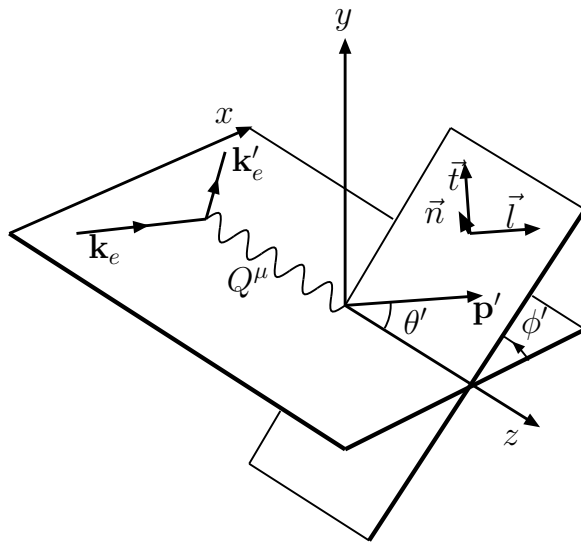


Figure 1: Kinematics and coordinate system used in this work. The  $x$ - $z$  coordinates span the scattering plane, while the ejected nucleon momentum  $\mathbf{p}'$  together with the momentum transfer ( $z$  direction) determines the reaction plane. The polarization vector  $\vec{s}$  of the nucleon is often referred to the barycentric coordinate system  $(\vec{l}, \vec{t}, \vec{n})$ , also shown in the figure, although for the results in the present work we use the Lab system, determined by the  $(x, y, z)$  coordinates.

of the hadronic tensor

$$W^{\mu\nu} = \frac{1}{K} \sum_{M_B} \overline{\sum_{M_A}} \langle \mathbf{p}' \vec{s}, B | J^\mu(\mathbf{q}) | A \rangle^* \langle \mathbf{p}' \vec{s}, B | J^\nu(\mathbf{q}) | A \rangle. \quad (6)$$

Here we average over third components of the angular momentum of the target ground state  $|A\rangle$  and sum over undetected orientations of the daughter nucleus in the (asymptotic) discrete state  $|B\rangle$ , for which we neglect recoil. The asymptotic nucleon state  $|\mathbf{p}' \vec{s}\rangle$ , with spin in the  $\vec{s}$  direction, is computed in DWIA as a solution of the Schrödinger equation with an optical potential. In the particular case of the results for  $^{40}\text{Ca}$  of the next section, we use the potential parameterization of Schwandt [40], the same considered in [25] since we want to compare with the results for polarized nuclei using the same interaction. The present model accounts for relativistic corrections that have proven to be successful in describing intermediate-energy inclusive and exclusive electron scattering observables in the region of the quasielastic peak [41, 42, 43, 44, 45]. First we use relativistic kinematics for the nucleons, as these are essential to have a correct description of the position and width of the quasielastic peak. Second we use the so-called semi-relativistic form of the nuclear (one-body) electromagnetic current operator,  $J^\mu(\mathbf{q})$ , obtained as an expansion in powers of  $\mathbf{p}/m_N$ , the missing momentum over the nucleon mass, maintaining the exact dependence on the energy-momentum transfer. The resulting semi-relativistic DWIA model (SR-DWIA) was applied to  $(e, e'p)$  reactions from polarized nuclei in [25, 26, 36], to recoil polarization observables in [11, 12], and to the unpolarized reaction in [35, 39, 41]. Effects beyond the impulse approximation due to meson-exchange currents (MEC) were discussed in [11, 12, 35] — it can be shown that they do not affect the results of the present work significantly.

The response functions in Eqs. (4,5) depend on the emission  $(\theta', \phi')$  and polarization  $(\theta_s, \phi_s)$  angles, apart from the kinematics. It is usual to extract the dependence on the azimuthal emission angle  $\phi' = \phi$ , where  $(\theta, \phi)$  are the polar angles of the missing momentum  $\mathbf{p} = \mathbf{p}' - \mathbf{q}$ . In this way one writes

$$R^L = W^L \quad (7)$$

$$R^T = W^T \quad (8)$$

$$R^{TL} = W^{TL} \cos \phi + \widetilde{W}^{TL} \sin \phi \quad (9)$$

$$R^{TT} = W^{TL} \cos 2\phi + \widetilde{W}^{TL} \sin 2\phi, \quad (10)$$

where the dependence of the six response functions  $W^K$  (with  $K = L, T, TL, TT$ ) and  $\widetilde{W}^K$  (with  $K = TL, TT$ ) on the azimuthal angles is now only via their difference  $\Delta\phi = \phi - \phi_s$ . In order also to display explicitly the spin-dependence ( $\vec{s}$ ) these response functions are expanded as sums of spin-scalar (0) plus spin-vector (V) response functions

$$W^K = W_0^K + W_V^K = \frac{1}{2} W_{\text{unpol}}^K + W_n^K s_n \quad K = L, T, TL, TT \quad (11)$$

$$\widetilde{W}^K = \widetilde{W}_V^K = W_l^K s_l + W_t^K s_t \quad K = TL, TT \quad (12)$$

where the scalar responses  $W_0^K$  are precisely one-half of the corresponding unpolarized response (since the sum over two possible final spin orientations of the nucleon cancels the factor 1/2). The vector responses have the form of a scalar product and have been written as a linear combination of the spin components in the barycentric system,  $(s_l, s_t, s_n)$ , where the coefficients in this expansion,  $W_i^K$ , are the so-called polarized reduced response functions. We can see from Eq. (11) that in the case of the responses without a tilde,  $W_V^K = W_n^K s_n$ , and only the normal component of the spin enters. The tilde responses, Eq. (12), are purely spin-vector; hence they are zero in absence of polarization and they have no normal component, *i.e.*, only the components of the spin in the reaction plane contribute. Expressions for the reduced response functions,  $W_i^K$ , using the present DWIA model were presented in [11] as a general multipole expansion, and in [39] for the case of the unpolarized ones,  $W_{\text{unpol}}^K$ .

Using the above-defined sets of response functions, the cross section in Eq. (1) can be expanded as the sum of spin-scalar plus spin-vector parts

$$\Sigma = \Sigma_0 + \Sigma_V = \frac{1}{2}\Sigma_{\text{unpol}} + \Sigma_V, \quad (13)$$

where  $\Sigma_{\text{unpol}} = 2\Sigma_0$  is the unpolarized cross section,

$$\Sigma_0 = K\sigma_M \left( v_L W_0^L + v_T W_0^T + v_{TL} W_0^{TL} \cos \phi + v_{TT} W_0^{TT} \cos 2\phi \right) \quad (14)$$

and the spin-vector part can be written as a scalar product, *i.e.*, in the barycentric system

$$\Sigma_V = \Sigma_l s_l + \Sigma_t s_t + \Sigma_n s_n \quad (15)$$

with

$$\Sigma_n = K\sigma_M \left( v_L W_n^L + v_T W_n^T + v_{TL} \cos \phi W_n^{TL} + v_{TT} \cos 2\phi W_n^{TT} \right) \quad (16)$$

$$\Sigma_l = K\sigma_M \left( v_{TL} \sin \phi W_l^{TL} + v_{TT} \sin 2\phi W_l^{TT} \right) \quad (17)$$

$$\Sigma_t = K\sigma_M \left( v_{TL} \sin \phi W_t^{TL} + v_{TT} \sin 2\phi W_t^{TT} \right). \quad (18)$$

Finally in terms of the polarization asymmetries we can write

$$\Sigma = \frac{1}{2}\Sigma_{\text{unpol}} (1 + \mathbf{P} \cdot \vec{s}), \quad (19)$$

where the induced polarization asymmetry vector,  $\mathbf{P}$ , has been introduced as the quotient between the spin-vector components and the spin-scalar cross section.

$$P_i = \Sigma_i / \Sigma_0, \quad i = n, l, t \quad (20)$$

The component of the polarization in a given direction  $\vec{s}$  can be obtained in a coincidence experiment as an asymmetry by measuring the number  $N(\vec{s})$  of protons polarized in the direction  $\vec{s}$  minus the number  $N(-\vec{s})$  of protons polarized in the  $-\vec{s}$  direction, divided by the sum

$$\mathbf{P} \cdot \vec{s} = \frac{N(\vec{s}) - N(-\vec{s})}{N(\vec{s}) + N(-\vec{s})} \quad (21)$$

and in this way in experimental studies one can minimize systematic errors contained in the separate polarized cross sections.

The roles of the various ingredients of our model (FSI, MEC, *etc.*) in the induced polarization components were analyzed in [11, 35] for selected quasielastic kinematics. The MEC effects were found to be negligible for missing momentum less than the Fermi momentum ( $\sim 240$  MeV/c), thereby corroborating our contention that the impulse approximation is appropriate for analyzing these observables under this kinematics.

In the following we show results for the cross section and related observables as functions of the missing momentum for various polarization directions.

## 3 Results

### 3.1 Cross section and semi-classical picture

In [25] the total cross section for  $(e, e'p)$  reactions from *polarized* nuclei was computed using the present SR-DWIA model and the results were analyzed in the light of a semi-classical model of the struck nucleon's orbit and mean free path of the final-state ejected nucleon. The analysis was later successfully extended to the case of polarized electrons [26]. In [25] different FSI effects were found for different initial polarization directions of the nucleus. This polarization dependence was analyzed within the context of the aforementioned semi-classical picture of the nucleon orbit. One of the goals of this section is to show the connections of the polarized nucleus case (*i.e.*, polarization of the initial state) with the case of nucleon recoil polarization (final state) and with what sometimes has been called the ‘‘Maris effect’’ in the literature [1, 3, 10]. We are interested in emphasizing the differences between the two reactions with respect to the physical information that can be obtained, and the advantages of one over the other from the theoretical point of view.

In order to proceed with this study it is convenient to express the recoil polarization observables in the Lab system  $(x, y, z)$  instead of the barycentric coordinates  $(l, t, n)$  used in the experimental studies. The latter are relative to the path of the final proton, and hence they depend on the emission angles, while the former are fixed with respect to the initial state, and therefore do not depend on the emission angles. Accordingly the Lab

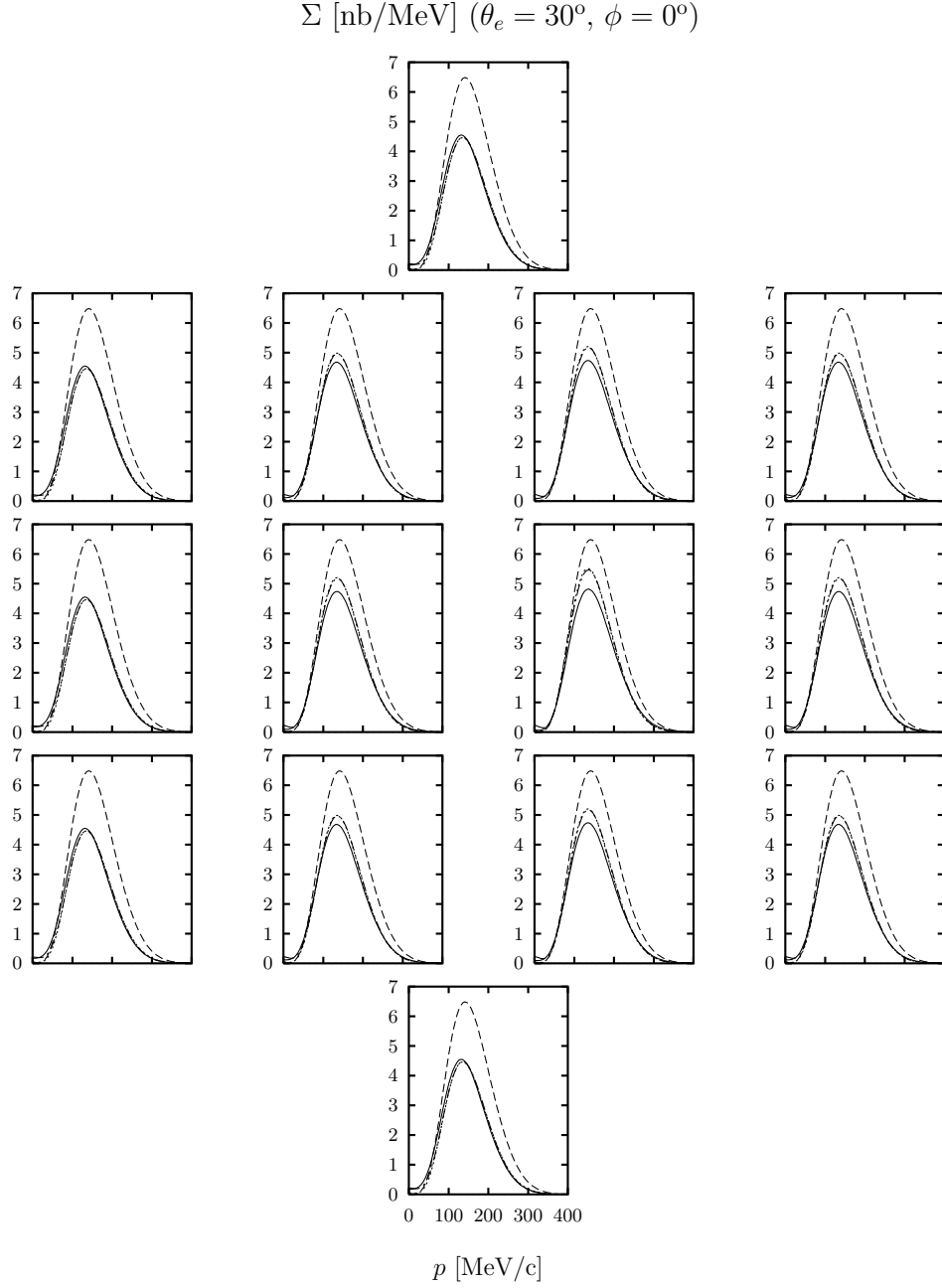


Figure 2: Proton knockout cross section from the  $d_{3/2}$  shell of  $^{40}\text{Ca}$  for  $q = 500$  MeV/c and  $\omega = 133.5$  MeV. Each panel corresponds to a different orientation of the final proton spin  $\vec{s}$ . From up to down,  $\theta_s = 0, 45^\circ, 90^\circ, 135^\circ, 180^\circ$ . From left to right, for  $\Delta\phi \equiv \phi - \phi_s = 0, 45^\circ, 90^\circ, \text{ and } 135^\circ$ . Dashed lines: PWIA. The rest of the curves are from DWIA calculations with the full optical potential (solid), with  $V_{ls} = 0$  (dot-dashed), and with  $\text{Re}V_C = V_{ls} = 0$  (dotted).

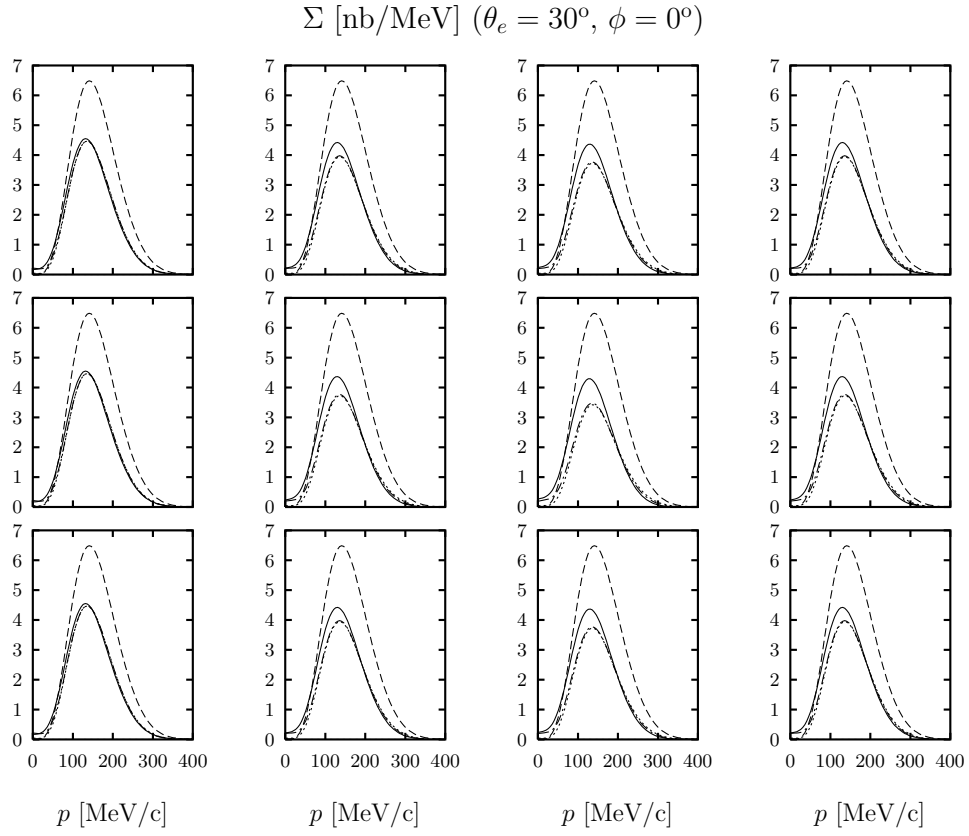


Figure 3: As for Fig. 10 for spin angles, from up to down,  $\theta_s = 45^\circ, 90^\circ, 135^\circ$ , and  $180^\circ$  and from left to right,  $\Delta\phi = 180^\circ, 225^\circ, 270^\circ$ , and  $315^\circ$ .

system is appropriate when one wishes to compare with the polarized target case and to relate the results with the corresponding nucleon orbit in the “initial” state.

Fixing on an explicit case for discussion, in Figs. 2 and 3 we show the cross section for proton knockout from the  $d_{3/2}$  shell of  $^{40}\text{Ca}$  for azimuthal angle  $\phi = 0$ . The various panels correspond to different final polarization angles,  $\theta_s$  and  $\Delta\phi \equiv \phi - \phi_s$  for the proton. Specifically, in Fig. 2 we show results for angles, from up to down panels,  $\theta_s = 0, 45^\circ, 90^\circ, 135^\circ, 180^\circ$ , and, from left to right, for  $\Delta\phi = 0, 45^\circ, 90^\circ, 135^\circ$ . Thus the results of Fig. 2 are a plot of the cross section for the “occidental” hemisphere in the space of polarization angles, including the north and south poles. The second “oriental” hemisphere is displayed in Fig. 3, where the chosen angles are, from up to down,  $\theta_s = 45^\circ, 90^\circ, 135^\circ$ , and  $180^\circ$ , and, from left to right,  $\Delta\phi = 180^\circ, 225^\circ, 270^\circ, 315^\circ$ . Note that in the figures the proton exits with  $\phi = 0$ . Hence  $\Delta\phi = -\phi_s$  for the present case.

The  $^{40}\text{Ca}$  nucleus has been chosen in order to make direct comparisons with the  $^{39}\text{K}$  polarized target considered in [25], where the initial state was described as a hole in the  $d_{3/2}$  shell of the  $^{40}\text{Ca}$  core. The kinematics  $q = 500 \text{ MeV}/c$ ,  $\omega = 133.5 \text{ MeV}$ , corresponding to the quasielastic peak, and  $\theta_e = 30^\circ$ , have also been chosen as in [25], where an expanded plot similar to Figs. 2 and 3 showing results for all of the nuclear polarization directions was also presented. This allows us to make direct comparisons with the present case, taking into account that the two sets of results correspond to different processes and the absolute values of cross sections are not the same, since there exist geometrical factors which depend on the polarization conditions. In particular, in [25] the case of knockout from the  $d_{3/2}$  shell of  $^{39}\text{K}$ , and two holes in the final state coupled to  $J_B = 0$  was considered. In [36], Eq. (82), it was demonstrated that the corresponding nuclear cross section is related to the one of a single polarized particle in the  $d_{3/2}$  shell, by a factor 1/2 for this particular case<sup>1</sup>.

To begin, we have checked the consistence of the calculation of [25] with the present results. Note that for the  $\phi = 0$  case considered in Figs. 2 and 3 the induced polarization has only a normal ( $n$ ) component; see Eqs. (16–18). Hence for  $\phi_s = \Delta\phi = 0$  (north and south poles and left-hand panels in Fig. 2) or  $\Delta\phi = 180^\circ$  (left-hand panels in Fig. 3) the induced polarization is zero and the  $^{40}\text{Ca}(e, e'p)$  unpolarized cross section must be recovered after multiplying by a factor of 2; see Eq. (19). Alternatively, note also that in PWIA (dashed lines) there is no induced polarization, and thus the dashed curves in all panels are identical.

Let us start the comparisons by restricting our attention to the PWIA results. By inspection in Fig. 2 we read a cross section at the maximum of roughly  $\Sigma \simeq 6.5 \text{ nb/MeV}$ . Hence the unpolarized cross section in PWIA is (see footnote)

$$\Sigma_{unpol} = 2\Sigma \simeq 13.0 \text{ nb/MeV} \simeq 260 \times 10^{-6} \text{ fm}^3. \quad (22)$$

---

<sup>1</sup>In [25] different units ( $\text{fm}^3$ ) were employed for the cross section and the relation  $1 \text{ nb/MeV} \simeq 20 \times 10^{-6} \text{ fm}^3$  must be applied before comparisons can easily be made.

Since there are four particles in the  $d_{3/2}$  shell, the unpolarized cross section per particle is

$$\frac{\Sigma_{unpol}}{4} \simeq 65 \times 10^{-6} \text{ fm}^3. \quad (23)$$

This number can be directly compared with the unpolarized cross section of  $^{39}\text{K}$  in PWIA, displayed with dashed lines in Fig. 3 of [25], which at the maximum is roughly  $\Sigma_{unpol} \simeq 32.5 \times 10^{-6} \text{ fm}^3$ . As stated earlier, this differs by a factor 1/2 from the unpolarized cross section for a particle, namely,  $\simeq 65/2 \times 10^{-6} \text{ fm}^3$ , in accordance with Eq. (23).

Next we discuss the effects that the FSI have on the nucleon polarization. These can be seen in Figs. 2 and 3 where we display the cross section from our DWIA model, showing the contribution of different terms of the optical potential

$$V_{\text{opt}}(r) = V_C(r) + V_{ls}(r)\boldsymbol{\sigma} \cdot \mathbf{L} = U_C(r) + iW_C(r) + [U_{ls}(r) + iW_{ls}(r)]\boldsymbol{\sigma} \cdot \mathbf{L}. \quad (24)$$

With solid lines we show the total DWIA calculation using the full potential. To be compared with this, with dot-dashed lines we show results after setting to zero the spin-orbit part of the optical potential ( $V_{ls} = 0$ ), while the dotted lines include only the imaginary part of the central optical potential (*i.e.*,  $V_{ls} = 0$ ,  $U_C = 0$ ). Finally the dashed lines do not include FSI (PWIA). Remember that the PWIA cross section (dashed lines) is the same for all of the polarizations, in accordance with the fact that there is no induced polarization in the absence of FSI.

First, note that the full FSI (compare the dashed with the solid lines) produces for all polarizations a reduction of the cross section in the region around the maximum of the momentum distribution for the chosen shell. Second, the magnitude of this reduction depends smoothly on the polarization direction and varies slowly throughout the various panels shown in the figures. Looking at a given pair of panels corresponding to opposite nucleon polarizations we see that in general the total cross section is different for the two polarizations. Under these conditions a net nucleon polarization component is generated along the given direction. The exception arises for the cases  $\Delta\phi = 0, 180^\circ$  spanning the  $xz$  plane (left-hand panels in the figures), since the normal direction, which is in fact the direction of the induced polarization vector  $\mathbf{P}$  for  $\phi = 0$ , has a zero component in the  $xz$  plane. Note also that the FSI reduction is in general more pronounced for the polarizations of Fig. 3 than for Fig. 2; this fact is related to the Maris effect and will be explained below. This determines the sign of the polarization component in a given direction.

Concerning the various ingredients of the FSI, we see that the imaginary part of the central optical potential,  $\text{Im}V_C$  (dotted lines), is the main one responsible for the reduction of the cross section due to the absorption effect. Note that this reduction is again stronger for the polarizations of Fig. 3 than for Fig. 2 (except for the  $\Delta\phi = 0, 180^\circ$  cases which do not depend on polarization). A larger reduction (around 50%) is found for the polarization

$\theta_s = 90^\circ$ ,  $\Delta\phi = 270^\circ$  in Fig. 3, while it is smaller ( $\sim 20\%$ ) for the opposite polarization  $\theta_s = 90^\circ$ ,  $\Delta\phi = 90^\circ$  in Fig. 2. If we also add the real part of the central optical potential,  $\text{Re}V_C$  (dot-dashed lines), producing only scattering, the cross section is almost unchanged. Finally, the inclusion of the spin-orbit part of the potential,  $V_{ls}$  (solid lines), produces an additional decrease (increase) of the cross sections of Fig. 2 (Fig. 3). This reduces the difference between cross sections for opposite polarization directions, *i.e.*, the spin-orbit interaction produces an effect that goes towards reducing the induced polarization.

Next we will focus our analysis on the FSI produced exclusively by the imaginary part of the optical potential (dotted lines in Figs. 2 and 3). Thus we disregard for the moment the effect of the spin-orbit part of the interaction which also affects the induced polarization, and which will be considered later.

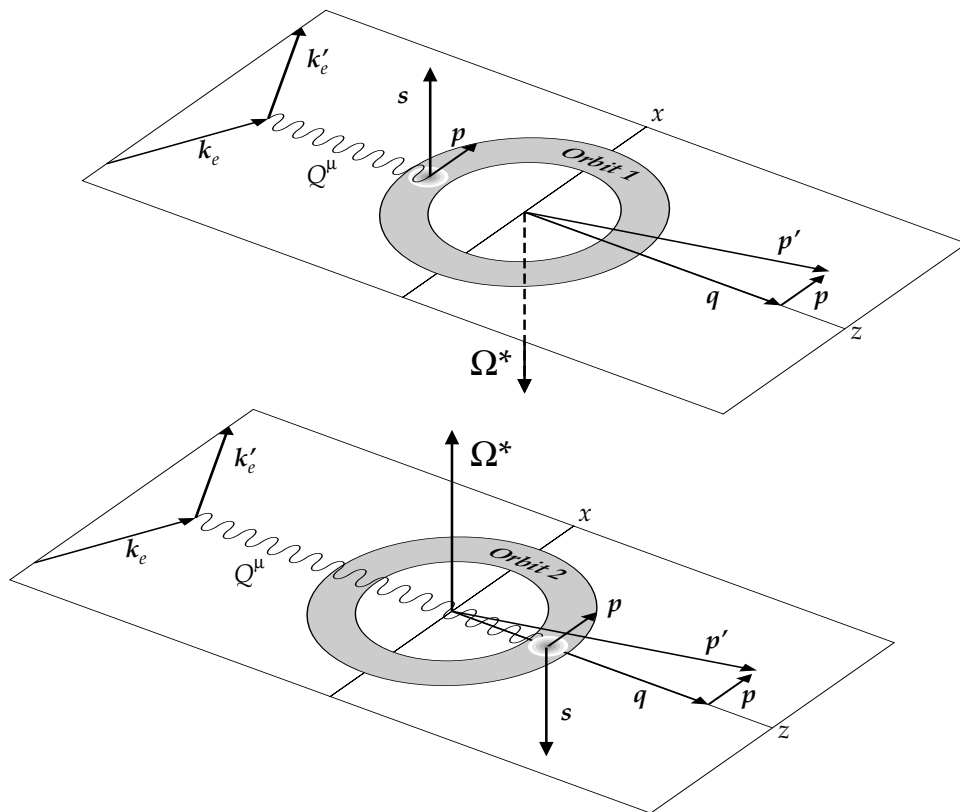


Figure 4: Semi-classical picture for opposite polarizations of the nucleon in a  $d_{3/2}$  orbit, for identical kinematical conditions. The expected position of the proton is indicated with a shaded ball.

The impact of the FSI as a function of the polarization seen in Figs. 2 and 3 is qualitatively similar to what was found in the case of polarized  $^{39}\text{K}$  in [25], where large absorption effects for some polarizations and small for the opposite were observed. These

properties of FSI for polarized nuclei were explained in [25] within the context of the semi-classical concept of nucleon orbit. Here we briefly discuss how that model can describe the present case of induced nucleon polarization. Focusing on the  $d_{3/2}$  case, we consider a particle in that orbit, initially polarized in the direction  $\boldsymbol{\Omega}^*$  (Fig. 4). Here the polarization of the orbit is the direction of the total angular momentum obtained as the vector sum of spin plus orbital angular momentum. In the jack-knifed case of a  $d_{3/2}$  wave one expects that the spin and orbital angular momentum be opposite. The spatial distribution of the proton can be pictured as a torus-like distribution, where the proton is rotating in a counter-clockwise sense with respect to the polarization direction of the orbit  $\boldsymbol{\Omega}^*$  (see Fig. 4). In fact the (local) expectation value of momentum at a position  $\mathbf{r}$  inside the  $d_{3/2}$  orbit is given in the semi-classical model by

$$\mathbf{p}(\mathbf{r}) = \frac{1 + \sin^2 \theta_r^*}{r^2 \sin^2 \theta_r^*} \boldsymbol{\Omega}^* \times \mathbf{r}, \quad (25)$$

corresponding to a rotational movement around the axis  $\boldsymbol{\Omega}^*$ , where  $\theta_r^*$  is the angle between  $\mathbf{r}$  and  $\boldsymbol{\Omega}^*$ . The angular dependence is determined by the geometry of the  $d_{3/2}$  wave. Going to momentum space, a dual expression can be obtained for the expected value of the proton position for a given momentum

$$\mathbf{r}(\mathbf{p}) = -\frac{1 + \sin^2 \theta_p^*}{r^2 \sin^2 \theta_p^*} \boldsymbol{\Omega}^* \times \mathbf{p}, \quad (26)$$

where now  $\theta_p$  is the angle between  $\boldsymbol{\Omega}^*$  and  $\mathbf{p}$ . This equation means that, given the orbit polarization direction  $\boldsymbol{\Omega}^*$  and the value of missing momentum  $\mathbf{p}$  (determined by the kinematics) one can compute the expected position of the proton inside the orbit, as displayed in the examples of Fig. 4. After the interaction with the virtual photon occurs, the proton exits the nucleus with momentum  $\mathbf{p}' = \mathbf{p} + \mathbf{q}$ . Since we know the initial position of the proton inside the nucleus, we can determine the amount of nuclear matter that the proton has to traverse before exiting, and this in turn determines the total absorption due to the imaginary part of the optical potential, *i.e.*, the reduction with respect to the PWIA cross section. This effect was analyzed in depth in [25].

In the case of nucleon recoil polarization of interest here, a second ingredient is the expectation value of the proton spin for momentum  $\mathbf{p}$  within the orbit, which is related to the spin density in momentum space [26]. The corresponding spin-direction field for the  $d_{3/2}$  shell was computed in [26] and is given by

$$\mathbf{s}(\mathbf{p}) = 2 \frac{\boldsymbol{\Omega}^* \cdot \mathbf{p}}{p^2} \mathbf{p} - \boldsymbol{\Omega}^*. \quad (27)$$

In particular, if  $\mathbf{p}$  is perpendicular to  $\boldsymbol{\Omega}^*$ , as in Fig. 4, then  $\mathbf{s} = -\boldsymbol{\Omega}^*$ , corresponding to spin opposite to the polarization direction, as expected for a  $d_{3/2}$  wave. The above equation can be inverted to obtain the orbit polarization as a function of the proton spin:

$$\boldsymbol{\Omega}^* = 2\frac{\mathbf{s} \cdot \mathbf{p}}{p^2}\mathbf{p} - \mathbf{s}. \quad (28)$$

Since the (detected) proton spin direction  $\vec{s}$  is known for all of the panels of Figs. 2 and 3, we can readily determine the corresponding orbit polarization direction  $\boldsymbol{\Omega}^*$  using Eq. (27), and therefore, from Eq. (26), also the proton position for each value of the missing momentum. This was done for the case of polarized  $^{39}\text{K}$  in [25, 26], where, from the nuclear transparencies computed as the quotient between PWIA and DWIA cross sections, it was possible to extract a theoretical value for the proton mean free path in our model.

As an example, in the simplest case of normal polarization we can have the two situations depicted in Fig. 4. Both correspond to in-plane ( $\phi = 0$ ) knockout of a proton for quasielastic kinematics; that is,  $p \simeq q$  and  $\mathbf{p}$  is almost perpendicular to  $\mathbf{q}$  (quasi-perpendicular kinematics). In both cases the proton is ejected from the  $d_{3/2}$  shell of  $^{40}\text{Ca}$ , and the corresponding orbit is represented by the shaded region as a planar projection. The only difference between the two cases is the direction of the initial spin. In the first case (top) the proton spin points upwards, with  $\theta_s = 90^\circ$  and  $\Delta\phi = -\phi_s = -90^\circ$ , corresponding to the panel in the second row and third column of Fig. 3. Here the initial proton is located in the half-plane with  $z$  negative, because it is following the orbit labeled “orbit 1” in Fig. 4 in clockwise sense. Since it is exiting the nucleus with momentum  $\mathbf{p}'$ , it has to cross the entire nucleus, which implies large absorption due to FSI along its path. This is why in Fig. 3 the FSI due to absorption is large (dotted lines). In contrast, for the opposite spin direction (bottom),  $\Delta\phi = 90^\circ$ , corresponding to the panel in the third row and third column in Fig. 2, the proton is following “orbit 2” in Fig. 4, in a counter-clockwise sense. Therefore the initial proton position is now in the positive  $z$  region, while its final momentum is the same,  $\mathbf{p}'$ , as before. Hence it has to cross only the nuclear surface along its path, implying small absorption due to FSI, in accord with the results of Fig. 2.

Thus the semi-classical picture that was able to explain FSI effects due to absorption in  $(e, e'p)$  reactions from polarized nuclei (at least in proton knockout from the valence shell and for low missing momentum) is also consistent with the case considered here of recoil polarization. This demonstration is the main goal of this work and clearly provides a connection between the two kinds of reactions, implying that both are consistent from this point of view. We have shown that the mechanism that connects FSI with target polarization in one reaction is the same one that induces recoil polarization in the other. However there are also quantitative differences between the FSI effects in the two processes. Namely, for the polarizations for which FSI is large (Fig. 3) the effect is not as pronounced as in the case of a polarized nucleus (Fig. 1 of [25]). In other words the

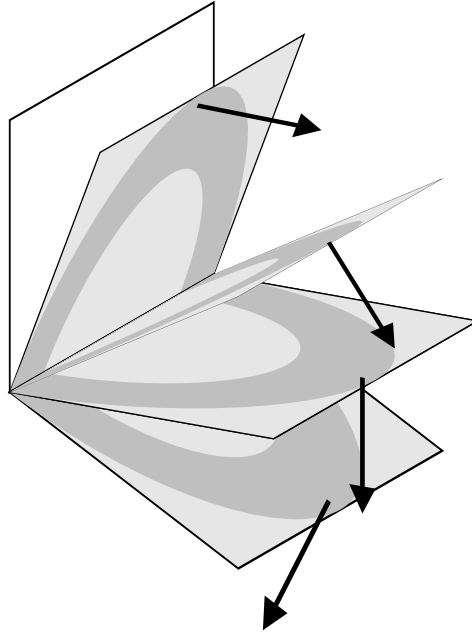


Figure 5: Example of different orbits for which the initial proton has non-zero spin projection in the normal direction.

maximum reduction due to FSI is larger for the polarized target case than for the recoil polarization case. The opposite happens for the cases where the FSI is small (Fig. 2), *i.e.*, the minimum reduction due to FSI is smaller for the polarized target case than for the recoil polarization case (compare with Fig. 2 of [25]).

The reason for these differences is of a basic quantum nature related to the different kinds of measurements involved in the two reactions, since in one case the polarization refers to the initial state, while in the other it is the final state that is polarized. Indeed, in the case of polarized target the system is initially prepared in a state polarized in a given direction (we assume 100% polarization here); hence the orbit is uniquely determined, as in the semi-classical picture in Fig. 4 for instance. In the case of recoil polarization, one measures the polarization of the proton in a given direction  $\vec{s}$  as the projection over the state  $|\mathbf{p}\vec{s}\rangle$ ; however, there are many spin directions that have non-zero projections in the direction  $\vec{s}$ . In other words, the final state is not fully polarized in one direction before the measurement. This is, of course, related to a fundamental postulate of quantum theory; only *after* the measurement can one assure that the proton is polarized. Therefore within the semi-classical picture, there are many possible initial orbits for the initial proton with spin direction having a non-zero projection in the direction of measurement,  $\vec{s}$ . In the example of Fig. 4, rotations of the initial orbit, as shown schematically in Fig. 5, give a net

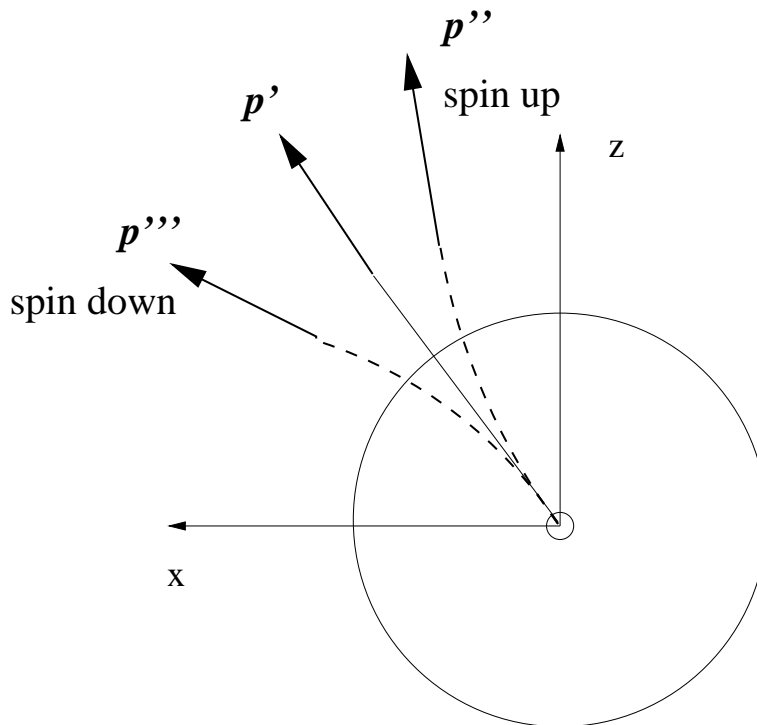


Figure 6: Deviations of ejected proton trajectories due to the real part of the spin-orbit potential for spin-up and spin-down polarizations (see Fig. 4 for kinematics).

spin projection in the normal direction. Hence all of the orbits of Fig. 5 contribute to the final cross section, with a weighting proportional to the cosine of the angle. Since these orbits imply different initial positions for the proton, and therefore different magnitudes for the FSI effects, the final cross section that results is an average between cases where FSI is large and other where it is not so large. Accordingly, the magnitude of FSI in the results of Figs. 2 and 3 can be understood as average values coming from the different polarizations in the final state, or as average values of the FSI effects found in the polarized target case of [25].

We should add that this implies a fundamental difference between polarized target and recoil polarization reactions. In the first case the net polarization could reach 100%, at least theoretically. In the second case is not possible to have 100% polarization in the final state before the measurement. In this sense, the physical information that can be obtained in reactions with polarized targets will be always richer than that obtained with the recoil polarization reactions that unavoidably contain polarization averages.

Up to now we have centered our attention on the imaginary part of the optical potential which gives the major effect for the cross section results of Figs. 2 and 3. The remaining effect is mainly produced by the real part of the spin-orbit potential. In [1] a semi-

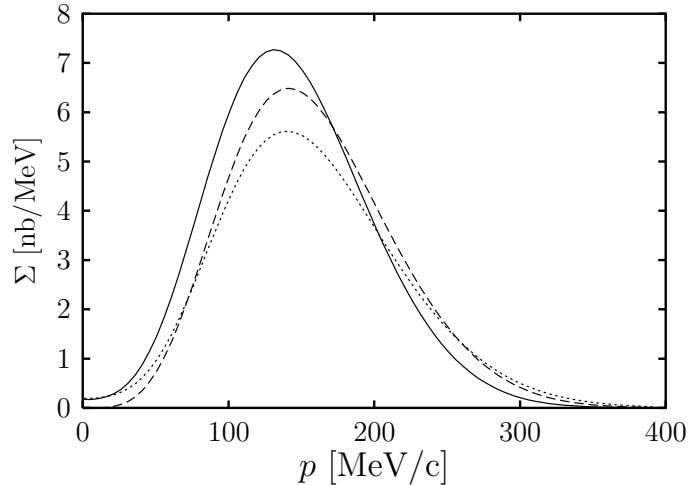


Figure 7: Cross section for proton knockout from the  $d_{3/2}$  shell of  $^{40}\text{Ca}$  with electron scattering angle  $\theta_e = 30^\circ$  and  $\phi = 0$ . The DWIA calculations include only the real part of the spin-orbit in the optical potential for spin-up (normal direction  $\vec{n}$ , solid lines) and spin-down ( $-\vec{n}$  direction, dotted lines) polarized protons. The PWIA is shown with dashed lines. The spin-up distribution is shifted to the left of the spin-down one.

classical argument was used to justify the sign of the induced polarization measured in  $^{12}\text{C}$ . Following [1] the spin-orbit force can be written

$$\mathbf{F} = -\nabla [V_{ls}(r)\boldsymbol{\sigma} \cdot \mathbf{L}] = -\hat{\mathbf{r}} \frac{dV_{ls}}{dr} \boldsymbol{\sigma} \cdot \mathbf{L} + V_{ls} \boldsymbol{\sigma} \times \mathbf{p}'. \quad (29)$$

Let us consider the case of  $\phi = 0$  and normal polarization  $\vec{s} = \pm\vec{n}$ . Assuming  $V_{ls} < 0$  and constant, the effect of the second term in Eq. (29) is to rotate the trajectory, with a force  $\mathbf{F} \propto \mathbf{p}' \times \vec{s}$ . This is shown schematically in Fig. 6, where a nucleon is emitted with final momentum  $\mathbf{p}'$ , and spin polarization pointing in the direction normal to the plane of the figure. The final momentum changes due to the spin-orbit force, in such a way that nucleons with spin up (pointing out of the plane) are shifted to its right, *i.e.*, to smaller angles from  $\mathbf{q}$ , while nucleons with spin down (pointing into the plane) are shifted to its left, *i.e.*, to larger angles. In other words, the missing momentum of nucleons with spin up decreases, while that of nucleons with spin down increases, and hence one should expect a shift of the missing momentum distribution of nucleons with spin up to the left of that for nucleons with spin down.

Such a shift can be verified from our DWIA results in Fig. 7, where we show the total cross section for protons polarized in the  $\pm\vec{n}$  directions for the same kinematics as Figs. 2 and 3, but including only the real part of the spin-orbit in the optical potential. The solid lines correspond to normal up polarization, and the dotted lines to the opposite

polarization. In the figure we can see the shift between the two distributions as suggested by the semi-classical argument. However, it is also clear that the difference between the two polarizations is not only a shift, but also that the maximum of the cross section for  $\vec{n}$  polarization is bigger than for  $-\vec{n}$  polarization. This should be related to the first term neglected in Eq. (29) that goes to increase or decrease the final momentum depending on the polarization and on the gradient of the spin-orbit potential. The net effect is not easy to depict in geometrical terms. In the figure we also show for comparison the PWIA cross section (dashed lines), which does not depend on polarization. Moreover, upon comparing with these PWIA results, we see that only the spin-up distribution is clearly shifted (to the left), while the position of the spin-down distribution is basically the same as the PWIA one.

### 3.2 Other polarization observables

To complete our discussion, in Figs. 8 and 9 we present results for observables other than the cross section. In Fig. 8 the separate response functions contributing to the cross section of Figs. 2 and 3 are shown for three directions of proton polarization: the  $-\vec{n}$  polarization (upper panels), corresponding to the panel  $\theta_s = 90^\circ$  and  $\Delta\phi = 90^\circ$  of Fig. 2;  $\vec{n}$  polarization (middle panels) corresponding to the panel  $\theta_s = 90^\circ$  and  $\Delta\phi = 270^\circ$  of Fig. 3; and finally polarization in the  $z$  direction (lower panels), corresponding to the case  $\theta_s = 0$  of Fig. 2. Since the azimuthal angle is  $\phi = 0$ , the responses  $\widetilde{W}^{TL}$  and  $\widetilde{W}^{TT}$  do not contribute to this cross section (see Eqs. (7–10)). For the same reason, the responses for  $z$ -polarization and  $\phi = 0$  do not have contributions from the spin-vector part (see Eq. (11)) and are identical to the unpolarized responses except for a factor 1/2. Figure 8 is complemented with Fig. 9, where for  $-\vec{n}$  polarization we show the vector part  $W_V^K$  of the response functions of Fig. 8 (see Eq. (11)). This contribution is precisely the difference between the upper and lower panels of Fig. 8, and also the difference between the lower and middle panels. These responses could in principle be extracted from experiment by performing a super-Rosenbluth plot for different kinematics.

The results of Fig. 8 illustrate the varied effects that the FSI have on the different responses when viewed as functions of the polarization. First we note that differences already exist between the L and T responses. For the L response the effect of the central imaginary part of the optical potential,  $W_C$ , is similar to the one found for the cross section: it is a small reduction for  $-\vec{n}$  polarization and large for  $\vec{n}$  polarization. However, in the case of the T response, this effect is basically the same for all of the polarizations. The reason can be deduced by examining Fig. 9, where  $W_V^T$  is almost zero if only  $W_C$  is included, while  $W_V^L$  is large in that case. This different behavior is related to the fact that the vector responses are zero in the absence of FSI, and to the different spin dependence of the L and T components of the electromagnetic current operator. The effect of  $W_C$  on the TL response,  $W_V^{TL}$ , has a similar behavior to that on the L response, being a small reduction for  $-\vec{n}$  polarization, and large for  $\vec{n}$  polarization (Fig. 8). This is because the vector response  $W_V^{TL}$  is approximately proportional to  $W_V^L$ , with a factor

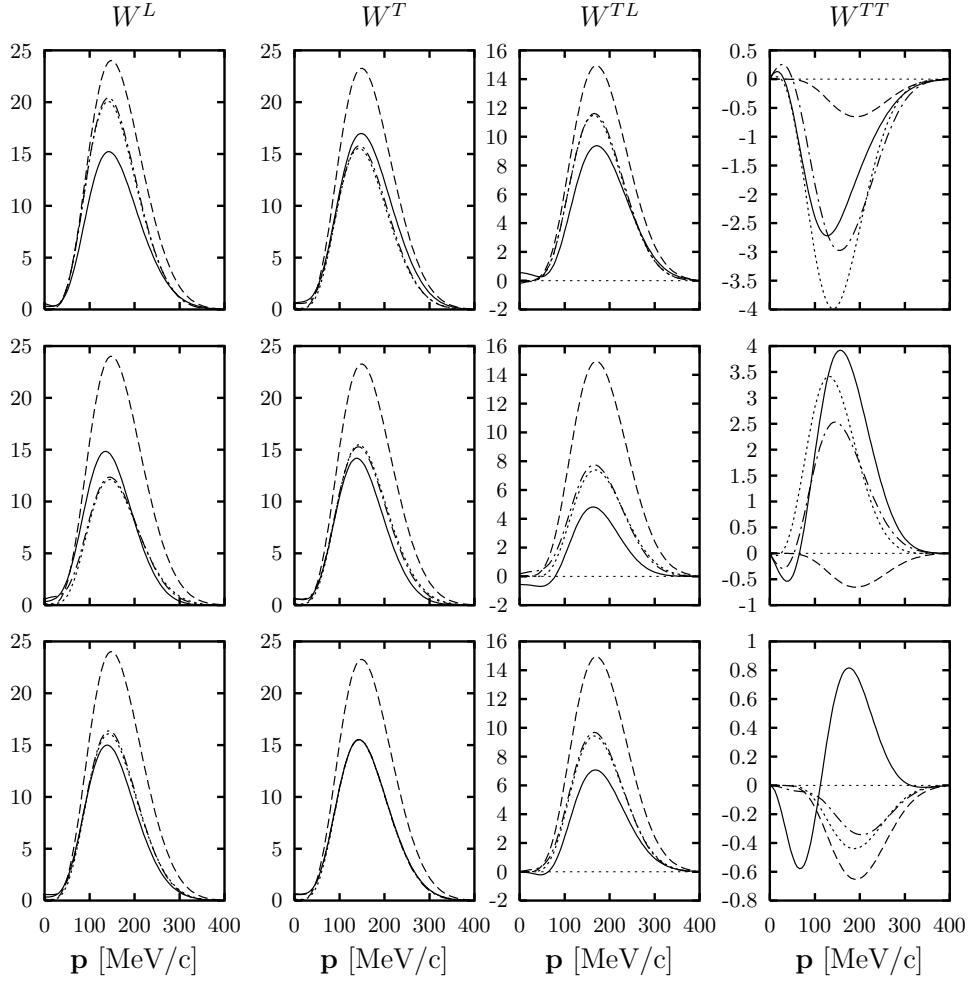


Figure 8: Separate response functions in units of  $\text{fm}^3$  for proton knockout from the  $d_{3/2}$  shell of  $^{40}\text{Ca}$ . The kinematics are the same as in Figs. 2 and 3. We show results corresponding to two different polarization directions for the recoil proton. Upper panels: proton polarized in the  $-\vec{n}$  direction ( $\theta_s = 90^\circ$ ,  $\Delta\phi = 90^\circ$ ). Middle panels: polarized in the  $\vec{n}$  direction ( $\theta_s = 90^\circ$ ,  $\Delta\phi = -90^\circ$ ). Lower panels: polarized in the  $z$ -direction,  $\theta_s = 0^\circ$ .

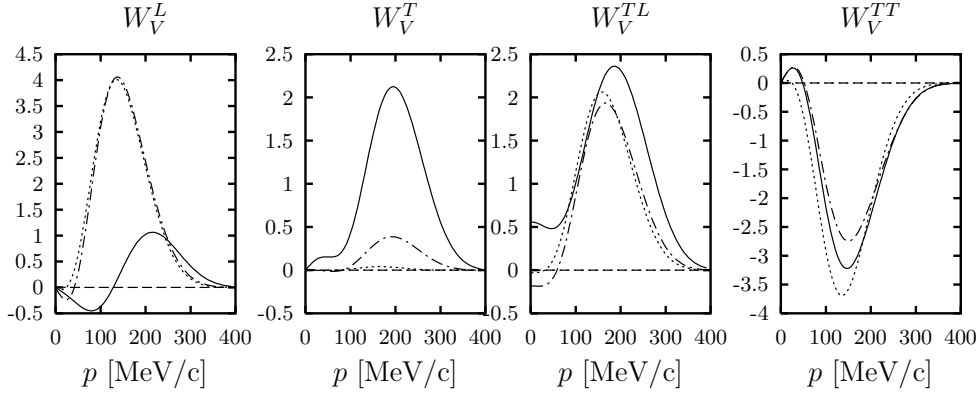


Figure 9: Vector parts of the separate response functions of Fig. 8 for  $-\vec{n}$  polarization

1/2, when only the  $W_C$  potential is used in the calculation (Fig. 9). The case of the TT response is different from the others because in PWIA this response is very small compared with them (in fact, it is exactly zero to first order in an expansion in powers of  $p/m_N$ ). Moreover, the unpolarized TT response (bottom panel in Fig. 8) is still small when FSI are included. However, the effect of FSI is amplified in the polarized case when we approach the  $\pm\vec{n}$  polarization. The size of this response changes dramatically (almost an order of magnitude) when the optical potential is included, and this effect is dominated by the imaginary central part,  $W_C$ . In fact, from Fig. 9, we see that the response  $W_V^{TT}$  for  $-\vec{n}$  polarization is of the same magnitude as the other three vector responses, or even larger when the full FSI is included. Concerning the real part of the central optical potential, it has a very small effect on these observables.

The spin-orbit potential has a different impact. It produces a large reduction of  $W_V^L$  (Fig. 9) in such a way that this vector response is close to zero near the peak of the momentum distribution, and hence the final polarized L response changes very slightly with the polarization angles (Fig. 8). The spin-orbit potential also has a large effect on the  $W_V^T$  response (Fig. 9), which is almost zero in absence of  $V_{ls}$ . On the other hand, the contribution of  $V_{ls}$  to the  $W^{TL}$  response is already large in the unpolarized case; however, this potential provides a small contribution to  $W_V^{TL}$ . The net effect of FSI on the  $T$  and  $TL$  responses is to produce a reduction which is smaller for  $-\vec{n}$  than for  $\vec{n}$  polarization. Finally, a very large effect of FSI is seen in the TT response, which even changes sign in going from  $-\vec{n}$  to  $\vec{n}$  polarization. The spin-orbit potential also produces a small effect on the  $W_V^{TT}$  response. All of the various effects seen in Figs. 8 and 9 coming from FSI interplay to produce the results of Figs. 2 and 3.

To finish, in Fig. 10 we show for the same kinematics other observables of interest that can be extracted from the results of Figs. 2 and 3. The left-hand panel contains the vector part of the cross section,  $\Sigma_V$ , for  $-\vec{n}$  polarization. This can be obtained as the difference between the corresponding cross section for  $-\vec{n}$  polarization and the upper

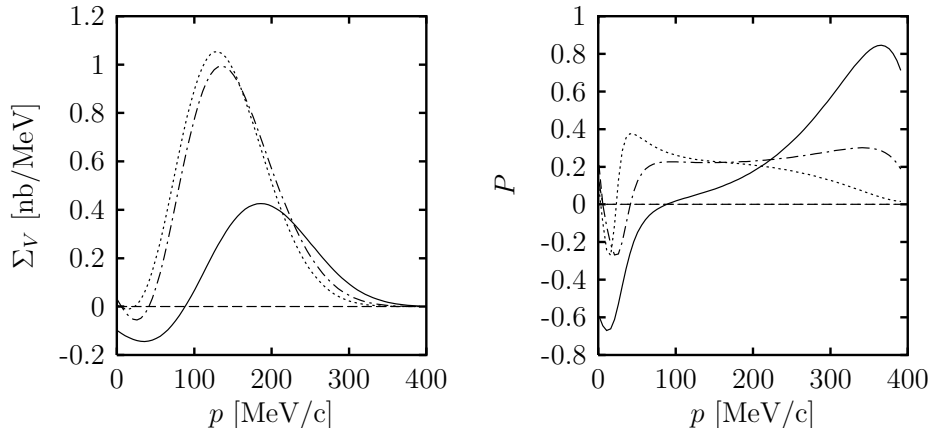


Figure 10: Vector part of the cross section and induced polarization in the  $-\vec{n}$  direction for the same kinematics as in Fig. 2.

panel in Fig. 2. In the right-hand panel we show the induced polarization also in the  $-\vec{n}$  direction. In this figure we can see again the contribution of the central parts of the potential and the full DWIA calculation. The spin-orbit potential reduces both  $\Sigma_V$  and  $P$  for low and intermediate missing momentum and increases the induced polarization for high  $p$ . The large values of the induced polarization for high missing momentum ( $P \sim 0.8$  for  $p > 300$  MeV/c) has also been predicted in previous work [1, 10, 12], but in this region other reaction mechanisms are also important, such as MEC or dynamical relativistic effects.

## 4 Conclusions

In this work we have performed a thorough study of polarization observables in exclusive  $(e, e'\vec{p})$  reactions leading to discrete residual nucleus states. We have used a semi-relativistic DWIA model including relativistic corrections to the one-body current as well as relativistic kinematics. Our model was successfully confronted with the available experimental data for polarization observables in [11, 12]. In the present work we have applied our approach to proton knockout from the outer shell of  $^{40}\text{Ca}$  for quasielastic kinematics and in-plane emission. We have focused on the dependence of the final-state interaction on the polarization angles. In this way we have been able to identify the polarization directions for which the FSI effects are large or small. This dependence has been compared with the findings of [25] for a polarized  $^{39}\text{K}$  nucleus, where the effects arising from the central imaginary part of the optical potential were explained using a semi-classical model based on the location of the proton in the orbit.

In this paper we have shown that the same semi-classical model is also able to explain the results of recoil polarization, using the relationship between polarization of the orbit

and expectation value of the spin. However, we have also found quantitative differences between FSI for the two reactions. For recoil polarization, the FSI effects present a softer dependence on the polarization angles. An explanation for this fact has been proposed by calling on the measurement postulate of quantum mechanics: in the case of recoil polarization the final proton is not really polarized before the measurement. Hence the initial orbit of the proton cannot be completely fixed, since there are other possible orientations giving a projection of the proton spin on the measurement direction, and all of these orbits contribute in a different way to the FSI. Thus the semi-classical orbit only determines the most probable orientation of the proton.

We have ended this paper by analyzing the separate response functions and other polarization observables for selected polarization angles, emphasizing the different sensitivities to the various contributions of the FSI. The case of the spin-vector part of the response functions for normal polarization is especially instructive, since these observables exhibit the strongest influences from the interaction, and hence their determination would place strong constraints on any theoretical calculation.

Differences between polarized target and recoil polarization arise irrespective of the underlying dynamics used. This is reminiscent of what is seen for the various polarization observables that contribute to the two types of reactions. In this sense, these two reactions are complementary to one another, and both are needed if one wants to extract all of the information available in the general case of exclusive reactions.

The unified picture that emerges from the present comparison between polarized target and recoil polarization is a good starting point to understand in an intuitive way how the underlying nuclear dynamics interact with the polarization degrees of freedom and affect the cross section for different polarizations. Thus, even if the complexity of full sets of polarization observables has not stimulated more experimental and theoretical research, we hope that the comprehensive view that we are reaching about polarization observables in these reactions encourage further studies in this field.

## Acknowledgments

This work was partially supported by funds provided by DGI (Spain) and FEDER funds, under Contracts Nos BFM2002-03218, BFM2002-03315 and FPA2002-04181-C04-04 and by the Junta de Andalucía. It was also supported in part (TWD) by the U.S. Department of Energy under cooperative agreement No. DE-FC02-94ER40818.

## References

- [1] R.J. Woo *et al.*, Phys. Rev. Lett. **80** (1998) 456.

- [2] S. Malov *et al.*, Phys. Rev. C **62** (2000) 057302.
- [3] J. J. Kelly, Adv. Nucl. Phys. **23** (1996) 75.
- [4] S. Boffi, C. Giusti, F. D. Pacati, and M. Radici, *Electromagnetic response of atomic nuclei*, Oxford University Press (1996).
- [5] H. Ito, S.E. Koonin, and R. Seki, Phys. Rev. C **56** (1997) 3231.
- [6] J. Ryckebusch, D. Debruyne, W. Van Nespen, and S. Janssen, Phys. Rev. C **60** (1999) 034604.
- [7] J.J. Kelly, Phys. Rev. C **59** (1999) 3256.
- [8] J.J. Kelly, Phys. Rev. C **60** (1999) 044609.
- [9] J.I. Johanson and H.S. Sherif, Phys. Rev. C **59** (1999) 3481.
- [10] J.M. Udías and J.R. Vignote, Phys. Rev. C **62** (2000) 034302.
- [11] F. Kazemi Tabatabaei, J.E. Amaro, and J.A. Caballero, Phys. Rev. C **68** (2003) 034611.
- [12] F. Kazemi Tabatabaei, J.E. Amaro, and J.A. Caballero, Phys. Rev. C **69** (2004) 064607.
- [13] M.C. Martínez, J.A. Caballero, and T.W. Donnelly, Nucl. Phys. A **707** (2002) 83.
- [14] M.C. Martínez, J.A. Caballero, and T.W. Donnelly, Nucl. Phys. A **707** (2002) 121.
- [15] M.C. Martínez, J.R. Vignote, J.A. Caballero, T.W. Donnelly, E. Moya de Guerra, and J.M. Udías, Phys. Rev. C **69** (2004) 034604.
- [16] J.R. Vignote, M.C. Martínez, J.A. Caballero, E. Moya de Guerra, and J.M. Udías, Phys. Rev. C **70** (2004) 044608.
- [17] S. Dieterich *et al.*, Phys. Lett. B **500** (2001) 47.
- [18] S. Strauch *et al.*, Phys. Rev. Lett. **91** (2003) 052301.
- [19] S. Frullani and J. Mougey, Adv. Nucl. Phys. **14** (1984) 1.
- [20] A.S. Raskin and T.W. Donnelly, Ann. Phys. (N.Y.) **191** (1989) 78.
- [21] S. Boffi, C. Giusti, and F.D. Pacati, Phys. Rep. **226** (1993) 1.
- [22] H.C. News, Proc. Phys. Soc. London Sect. A **66** (1953) 477.

- [23] H.C. News and M.Y. Refai, Proc. Phys. Soc. London Sect. A **71** (1958) 627.
- [24] G. Jacob, Th. A.J. Maris, C. Schneider, and M.R. Teodoro, Nucl. Phys. A **257** (1976) 517.
- [25] J.E. Amaro and T.W. Donnelly, Nucl. Phys. A **646** (1999) 187.
- [26] J.E. Amaro and T.W. Donnelly, Nucl. Phys. A **703** (2002) 541.
- [27] J.E. Amaro, M.B. Barbaro, and J.A. Caballero, nucl-th/0411043.
- [28] H. Arenhövel, W. Leidemann, and E.L. Tomusiak, nucl-th/0407053.
- [29] H. Arenhövel, W. Leidemann, and E.L. Tomusiak, Eur. Phys. Jou. A (2002) 491.
- [30] H. Arenhövel, W. Leidemann, and E.L. Tomusiak, Few Body Syst. **28** (2000) 147.
- [31] H. Arenhövel, W. Leidemann, and E.L. Tomusiak, Nucl.Phys. A **641** (1998) 517.
- [32] H. Arenhövel, W. Leidemann, and E.L. Tomusiak, Phys. Rev. C **52** (1995) 1232.
- [33] H. Arenhövel, W. Leidemann, and E.L. Tomusiak, Phys. Rec C **46** (1992) 455.
- [34] V. Dmitrasinovic and F. Gross, Phys. Rev. C **40** (1989) 2479.
- [35] J.E. Amaro, M.B. Barbaro, J.A. Caballero, and F. Kazemi Tabatabaei, Phys. Rev. C **68** (2003) 014604.
- [36] J.E. Amaro and T.W. Donnelly, Ann. Phys. (N.Y.) **263** (1998) 56.
- [37] A. Picklesimer and J.W. Van Orden, Phys. Rev. C **35** (1987) 266.
- [38] A. Picklesimer and J.W. Van Orden, Phys. Rev. C **40** (1989) 290.
- [39] M. Mazziotta, J.E. Amaro, and F. Arias de Saavedra, Phys. Rev. C **65** (2002) 034602.
- [40] P. Schwandt *et. al.*, Phys. Rev. C **26** (1982) 55.
- [41] J. M. Udías, J. A. Caballero, E. Moya de Guerra, J. E. Amaro, and T. W. Donnelly, Phys. Rev. Lett. **83** (1999) 5451.
- [42] J.E. Amaro, J.A. Caballero, T.W. Donnelly, E. Moya de Guerra, A.M. Lallena, and J.M. Udías, Nucl. Phys. A **602** (1996) 263.
- [43] J.E. Amaro, M.B. Barbaro, J.A. Caballero, T.W. Donnelly, and A. Molinari, Nucl. Phys. A **643** (1998) 349.
- [44] J.E. Amaro, M.B. Barbaro, J.A. Caballero, T.W. Donnelly, and A. Molinari, Phys. Rep. **368** (2002) 317.

- [45] J.E. Amaro, M.B. Barbaro, J.A. Caballero, T.W. Donnelly, and A. Molinari, Nucl. Phys. A **723** (2003) 181.